# Observation of Betatron X-Ray Radiation in a Self-Modulated Laser Wakefield Accelerator Driven with Picosecond Laser Pulses

F. Albert, N. Lemos, J. L. Shaw, B. B. Pollock, C. Goyon, W. Schumaker, A. M. Saunders, K. A. Marsh, A. Pak, J. E. Ralph, J. L. Martins, L. D. Amorim, R. W. Falcone, S. H. Glenzer, J. D. Moody, and C. Joshi

Phys. Rev. Lett. **118**, 134801 — Published 31 March 2017

DOI: 10.1103/PhysRevLett.118.134801

# Observation of betatron x-ray radiation in a self-modulated laser wakefield accelerator driven with picosecond laser pulses

F. Albert[1,*], N. Lemos[1,2], J. L. Shaw[2,**], B. B. Pollock[1], C. Goyon[1], W. Schumaker[3], A. M. Saunders[4], K. A. Marsh[2], A. Pak[1], J. E. Ralph[1], J. L. Martins[5], L. D. Amorim[2,5], R. W. Falcone[4], S. H. Glenzer[3], J. D. Moody[1], and C. Joshi[2]

[1] *Lawrence Livermore National Laboratory, NIF and Photon Sciences, 7000 East Avenue, Livermore, California 94550, USA*

[2] *Department of Electrical Engineering, University of California, Los Angeles, California 90095, USA*

[3] *SLAC National Accelerator Laboratory, Stanford, California 94309, USA*

[4] *Lawrence Berkeley National Laboratory and University of California Berkeley, California, USA*

[5] *GoLP/Instituto de Plasmas e Fusão Nuclear, Instituto Superior Técnico, Universidade de Lisboa, 1049-001 Lisbon, Portugal*

We investigate a new regime for betatron x-ray emission that utilizes kilojoule-class, picosecond lasers to drive wakes in plasmas. When such laser pulses with intensities of $\sim 5 \times 10^{18}$ W/cm$^2$ are focused into plasmas with electron densities of $\sim 1 \times 10^{19}$ cm$^{-3}$, they undergo self-modulation and channeling, which accelerates electrons up to 200 MeV energies and causes those electrons to emit x-rays. The measured x-ray spectra are fit with a synchrotron spectrum with a critical energy of 10-20 keV, and 2D PIC simulations were used to model the acceleration and radiation of the electrons in our experimental conditions.

A frequently used method to probe the size, density and composition of highly-transient states of matter is x-ray backlighting using laser-produced x-rays. A source based on betatron emission from a laser-plasma accelerator [1] is attractive for this purpose because it generates a small-divergence, broadband x-ray beam that can be used to backlight the target being studied. Betatron x-ray radiation has been used for biological and medical purposes, such as x-ray phase contrast imaging of insects [2–4] and hard x-ray radiography of bone [5]. Its unique properties also make it suitable for studying the dynamics of high-energy-density plasmas and warm dense matter, a state near solid densities and a few electronvolts (eV) temperatures found in the core of jovian planets and inertial confinement fusion plasmas [6, 7]. Within this context, measurements that could possibly be made using a betatron x-ray source include x-ray radiography and phase contrast imaging of laser-driven shocks, near edge absorption spectroscopy, and opacity [8].

Most of the current work on betatron sources uses <50 fs-long laser pulses [1]. However, national large-scale laser facilities, where betatron radiation could serve as a backlighter x-ray beam, have kilojoule-class, picosecond lasers. Examples include the advanced radiographic capability (ARC) of the National Ignition Facility (NIF), the Petawatt Aquitaine Laser (PETAL) of the Laser Megajoule (LMJ) in France, and the LFEX laser at the University of Osaka in Japan. Initially, the peak intensities produced by these lasers are expected to be in the few times $10^{18}$ W/cm$^2$ range. In view of its potential for applications, it is therefore important to investigate the mechanisms of betatron x-ray emission using a picosecond-class laser with such intensity, which corresponds to a peak normalized vector potential $a_0 = 8.5 \times 10^{-10} \lambda_0[\mu\text{m}] I_L^{1/2}[\text{W/cm}^2]$ of about 2, where $I_L$ and $\lambda_0$ are the laser intensity and central wavelength, respectively. In the blowout LWFA regime, the laser pulse length $c\tau$ with $\tau$ the laser pulse duration and $c$ the speed of light in vacuum, is about half of a plasma period $\lambda_p = 2\pi c/\omega_p$, whereas in the self-modulated laser wakefield acceleration (SMLWFA) regime, the laser pulse overlaps with several tens of plasma periods. Consequently, the electron charge trapped in SMLWFA can be about two orders of magnitude higher than in the blowout regime, and recent Particle-In-Cell (PIC) simulations suggest that for conditions relevant to the PETAL laser (kJ, ps), SMLWFA can enhance the betatron x-ray yield by a factor of 10-400 [9] compared to the blowout regime.

In this Letter, we report on the first observation of betatron x-ray radiation in the SMLWFA regime from an experiment where 1 ps laser pulses are focused onto an underdense target (at an electron density $n_e < n_c$, where $n_c$ is the critical density) to intensities corresponding to $1 < a_0 < 3$.

When a picosecond laser pulse is focused onto an underdense target at intensities below $10^{19}$ W/cm$^2$, electrons are accelerated through SMLWFA. Initially, some of the photons are forward scattered by thermal fluctuations in the plasma at the plasma frequency. Stimulated forward Raman scattering [10] and self modulation are parametric decay instabilities that occur during the interaction, where the incident electromagnetic wave ($\omega_0$, $\vec{k}_0$) decays into an electron plasma wave ($\omega_p$, $\vec{k}_p$), and scattered electromagnetic wave ($\omega_s$, $\vec{k}_s$). These processes obey frequency and wavenumber matching conditions $\omega_0 = \omega_s \pm m\omega_p$ and $\vec{k_0} = \vec{k_s} \pm m\vec{k_p}$, where $m$ is an integer. For $m > 1$, these instabilities modulate the laser at the plasma period. Hence, a large-amplitude, resonant plasma wave is driven [11], which traps and accelerates plasma electrons up to relativistic energies [12–14]. When a self-modulated wakefield is present, elec-

trons that are trapped in the wakefield can also gain energy from the DLA mechanism [15] if they overlap the drive laser [16, 17]. If the laser intensity is increased to above $10^{20}$ W/cm$^2$, almost all the electrons are expelled from the focal volume, creating a near hollow channel [18]. The SMLWFA structure no longer exists in this case, and electrons will be accelerated by DLA alone [19] and emit betatron x-rays [20].

To study betatron x-ray emission at the lower intensities relevant to upcoming, larger-scale laser facilities, we conducted an experiment at the Jupiter Laser Facility, Lawrence Livermore National Laboratory, with the Titan laser. Titan is a Nd:glass laser system that produces $0.7^{+0.3}_{-0.1}$ ps-long pulses at a wavelength of 1.053 $\mu$m with up to 150 J on target. In our configuration (Figure 1), the laser is focused onto a 3-mm supersonic gas jet with an f/10 off-axis parabola (OAP). This geometry produces focal spots of 29.6 $\pm$6.1 $\mu$m radius, measured at low laser power and containing 86% of the total laser energy ($a_0 \sim 3$). This spot is well fit with a Gaussian of dimensions 16.5 $\pm$ 3.2 $\mu$m in the vertical direction and 20.3 $\pm$ 3.3 $\mu$m in the horizontal direction ($1/e^2$ intensity radius). The gas composition for each shot could be varied from pure He to He/$N_2$ mixtures containing between 1 and 100% $N_2$ (by partial pressure). The electron density, measured with interferometry, is between 0.1 and 1.5$\times10^{19}$ cm$^{-3}$. An uncoated glass wedge reflects the laser light transmitted through the gas jet onto an imaging optical spectrometer (Acton SpectraPro) coupled with a visible CCD camera (Princeton PI-XIS) which records wavelengths from 0.5 to 1.2 $\mu$m. An example image is shown in Figure 1. The electrons, accelerated in the jet and propagating in the forward direction through a hole in the glass wedge, are deflected onto two image plates by a 0.42 Tesla permanent magnet. This spectrometer, described in detail in previous work [21], measures the electron energy and deflection from the laser axis, with fiducials placed between the two image plates. X-rays pass through 15 filter wedges, arranged as Ross pairs, and are detected using image plates. The image plates are outside of the target chamber behind a 200 $\mu$m mylar and a 22 $\mu$m aluminum window and in front of a stacked-image-plate spectrometer [22, 23] used as a second diagnostic to also measure x-ray yield produced during the experiment.

Electrons display an exponentially-decaying energy distribution (Figure 2 A), that extends out to between 250 and 300 MeV. For a range of electron densities within 0.5-1.5$\times10^{19}$ cm$^{-3}$, with laser energies around 150 J ($a_0 \sim 2.9$), the number of electrons $N_e$ per MeV can be approximated by a two-temperature distribution of the form $N_e \propto e^{-E/T_1} + be^{-E/T_2}$ with $13 < T_1 < 18$ MeV and $20 < T_2 < 50$ MeV. The corresponding transmitted laser spectra (Figure 2 B) show Raman satellites indicative of large-amplitude plasma waves and of plasma electrons not completely expelled by the laser pulse. The

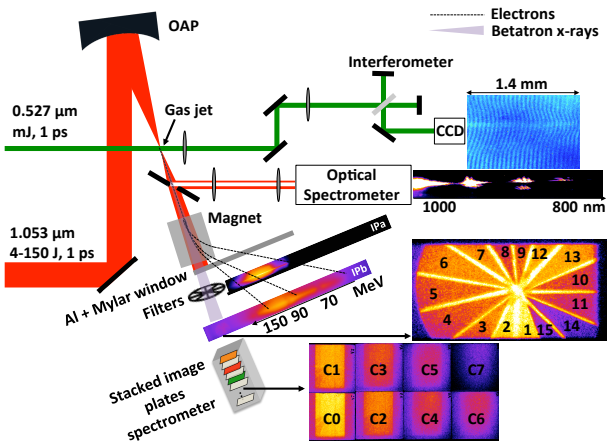


FIG. 1. Experimental setup, with the OAP focusing the laser pulse (red) on the gas jet, the transverse interferometry probe (green), and the transmitted laser optical spectrometer. An interferogram and transmitted laser spectrum are shown next to and below the interferometer CCD camera, respectively. The electrons (dashed line) are dispersed in energy by the magnet centered on the laser axis (122 cm from the source inside the target chamber) and recorded on image plates (IP$_a$ and IP$_b$), 167.5 cm and 187 cm away from the source, respectively. After exiting the vacuum chamber, x-rays (solid line) propagate through 15 wedge filters onto the image plates and then through an 8 channel stacked image plate spectrometer (see text for details). We show a raw image of IP$_a$ and IP$_b$, an enlarged image of the x-rays measured on the image plate through each of the 15 filters of the wheel, and the stacked image plate channels.

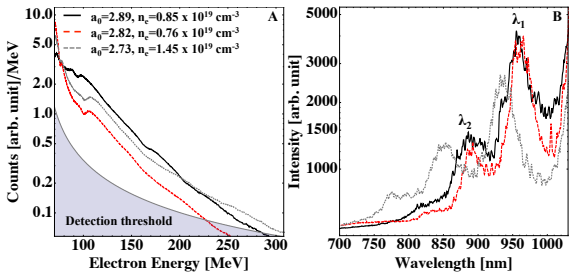


FIG. 2. (A) Measured electron beam spectra for different conditions, and (B) corresponding transmitted laser spectra, showing Raman anti-Stokes satellites ($\lambda_1$ and $\lambda_2$).

electron density and the relativistically-corrected plasma frequency $\omega_p$ are inferred from the position of two neighboring satellites with wavelengths $\lambda_1$ and $\lambda_2$ so that $\omega_p = \frac{2\pi c}{\lambda_2} - \frac{2\pi c}{\lambda_1}$. The electron densities measured here were consistent with those deduced from the interferometry to $\pm$30%.

The x-ray spectra contain both betatron from the SMLWFA and higher-energy Bremsstrahlung noise from electrons hitting the chamber. These are analyzed with two different methods. Both take into account the transmission of x-rays through elements of the system (Al, mylar windows) and the calibrated image plates absorption and efficiency [24]. For photon energies between 1

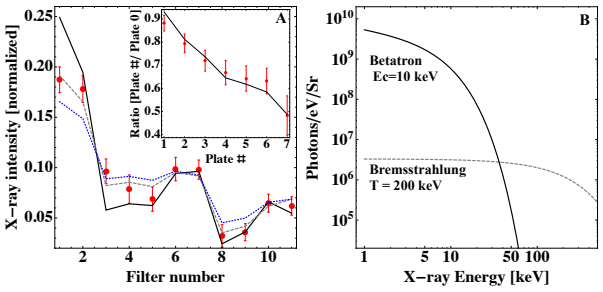


FIG. 3. (A) Normalized x-ray yield through filters of Figure 1 (red dots), for $a_0 = 3.05$ and $n_e = 10^{19}$ cm$^{-3}$, and critical energy fits calculated with Equation 1, with $E_c = 5$ keV, 10 keV and 15 keV (solid, dashed and dotted lines). Inset, stacked image plate data $R_{E,i}$ (red dots) and fit $R_{T,i}$ for a photon distribution (Equation 2) with $E_c = 10$ keV, A = 0.00014 and T = 200 keV. (B) Deduced betatron and Bremsstrahlung spectra (see text for details).

and 30 keV, we utilize the filter wheel. Assuming that the betatron motion of the electrons dominates the observed x-ray emission in this range, we consider an intensity distribution per unit photon energy $dE$ and solid angle $d\Omega$ as a function of the photon energy $E$ of the form:

$$\frac{d^2I}{dEd\Omega} \propto \left(\frac{E}{E_c}\right)^2 K_{2/3}^2[E/E_c], \qquad (1)$$

which is valid for betatron x-rays on axis [25]. Here $E_c$ is the critical energy of the betatron spectrum, and $K_{2/3}$ is a modified Bessel function. The distribution function is calculated through the different filters of the wheel and integrated to obtain the corresponding signal that it would yield on the image plate. The filters are sufficiently thin to neglect the effects of scattering for our range of energies. Both the experimental and theoretical data are normalized so that the sum of the signals of the filters is equal to 1. The data are analyzed through a least squares fitting method by minimizing the number $\sum_i (D_i - T_i)^2$, where $D_i$ and $T_i$ are, respectively, the measured and calculated normalized signals for each filter. One example is shown in Figure 3 A, for $a_0 = 3.05$ and $n_e = 10^{19}$ cm$^{-3}$. Here, the best fit is obtained for $E_c = 10$ keV. In our experimental conditions, the highest critical energy $E_c = 20$ keV was measured for $a_0 = 3.02$ and $n_e = 1.3 \times 10^{19}$ cm$^{-3}$. By differentiating the signal obtained in the Iron/Chromium Ross pair (filters 6 and 5, see image of Figure 1), we can deduce the x-ray photon yield $N_x$ at 6.5±0.5 keV. At constant electron density $n_e = 1.3 \times 10^{19}$ cm$^{-3}$, it goes from $N_x = 3 \times 10^8$ photons/eV.Sr for $a_0 = 1.44$ to $N_x = 1.45 \times 10^9$ photons/eV.Sr for $a_0 = 3.02$. A sharp, stainless-steel edge placed 22 cm from the source casts a clear shadow on the first image plate detector, indicating that for energies below 30 keV, the main source of x-rays originates at the gas jet, consistent with betatron emission. We do not expect any significant hard x-ray Bremsstrahlung emission from the very underdense plasma. The measured 1/e$^2$ source diameter has an upper value of 35 $\mu$m.

To quantify the x-ray spectrum at photon energies between 10 and 500 keV, we use the stacked image plate spectrometer. In addition to the betatron spectrum described by Equation 1, we assume an additional, high-energy photon background so that the total number of photons per unit energy on axis is:

$$\frac{dN_x}{dE} \propto \frac{1}{E}\left(\frac{E}{E_c}\right)^2 K_{2/3}^2[E/E_c] + A\exp[-E/E_T], \qquad (2)$$

where $E_T$ is the temperature of the exponentially-decaying Bremsstrahlung spectrum and $A$ its amplitude relative to the betatron spectrum. We propagate Equation 2 through the different materials of the experiment and through the calibrated stacked image plate spectrometer [23, 26]. The number $R_{T,i} = P_{T,0}/P_{T,i}$ is calculated, where $P_{T,0}$ is the total theoretical yield in the first plate (plate C0 in Figure 1) and $P_{T,i}$ the total theoretical yield in subsequent plates for $i = 1:7$. These values are compared to the experimental results $R_{E,i} = P_{E,0}/P_{E,i}$ to minimize the residue $\sum_i (R_{E,i} - R_{T,i})^2$ by varying the parameters $E_T$ and $A$. The betatron critical photon energy is set at $E_c = 10$ keV in agreement with the Ross pair filters measurements. The best fit (inset of Figure 3 A with the experimental data) is obtained for $E_T = 200$ keV and $A = 0.00014$. The residue is higher, by a factor of 10, if we fit using only betatron or Bremsstrahlung distributions separately. We deduce that the total x-ray yield observed in our experiment and shown in Figure 3 B is a combination of betatron radiation (dominant up to 40 keV) and Bremsstrahlung (dominant above 40 keV). The Bremsstrahlung, inevitable whenever relativistic electrons are produced, is likely due to lower energy ($< 500$ keV) electrons being strongly deflected by the magnet onto the walls of the target chamber.

To explain the observed betatron x-ray spectra, we performed 2D PIC simulations with OSIRIS for a variety of conditions [27]. We illustrate the salient observations from one simulation that uses an $a_0 = 3$, $\tau$=0.7 ps, $\lambda_0$=1.053 $\mu$m laser pulse focused to a spot size of 15 $\mu$m ($1/e^2$ intensity radius), into a 200 $\mu$m density up ramp. The pulse duration and $a_0$ were chosen to match the experimental values, and the spot size matches the value obtained from the Gaussian fit ($1/e^2$ intensity radius) of the measured spot. The pulse then propagates through a 3 mm-long fully-ionized helium plasma of constant electron density $n_e = 1 \times 10^{19}$ cm$^{-3}$. The simulation utilizes a moving window with box dimensions of 500 $\mu$m in the longitudinal (laser propagation) direction and 150 $\mu$m in the transverse direction. The corresponding resolutions are, respectively, 60 and 7.2 cells per $\lambda_0$. To calculate betatron x-ray emission in these conditions, we select 750 random electrons in energy to match the overall spectrum (Figure 4 C). The simulation is run again while

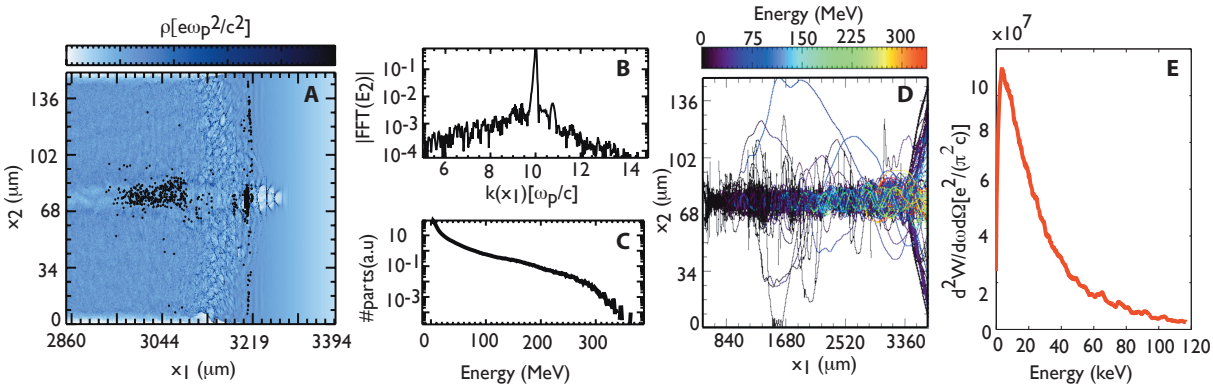


FIG. 4. Results of OSIRIS 2D PIC simulations. (A) electron density map at the beginning of the downramp, where the black dots represent the 750 tracked electrons. (B) Raman forward scattering spectrum, (C) Electron energy spectrum. (D) Trajectories of the 750 tracked electrons and energy gain throughout the simulation. (F) Overall betatron x-ray spectrum calculated with JRAD. See text for details of simulation.

also tracking the corresponding particles. Their position and momentum are used to calculate their emission with the post-processing code JRAD [28].

Figure 4 A shows the instantaneous electron density map after 3.2 mm of propagation through the plasma At $x_1 = 3200$ $\mu$m, we clearly see several plasma wave periods with length $\lambda_p$, consistent with the front of the laser pulse driving a large-amplitude plasma wave. In this region, electrons are mainly accelerated by the wakefield. At $x_1 = 3100$ $\mu$m, the back of the laser has expelled the electrons through relativistic self-focusing to form an ion channel. In this region, electrons are mainly accelerated by DLA [27], where, for our simulation parameters, DLA has been shown to be a physical effect and not a numerical artifact [29]. Figure 4 B shows the spectrum of the transmitted light. Here, as in the experiment, one can see the anti-Stokes satellite upshifted by the plasma frequency. Figure 4 C shows the electron spectrum at the end of the run. Again as in the experiment, an exponentially-decaying spectrum extending out to 300 MeV is observed. This spectrum is also best fit with a two-temperature Maxwellian distribution with $T_1 = 14$ MeV and $T_2 = 56$ MeV, similar to what is observed in the experiment. Figure 4 D shows the trajectories of the 750 tracked electrons. These electrons were randomly-chosen to represent the overall electron energy spectrum shown in 4 C and describe a strong betatron motion as they are accelerated in the plasma. Using JRAD, we calculated the betatron radiation spectrum emitted by these 750 electrons (Figure 4 E). Here, the x-ray photon energy below which 50% of all the radiated energy is contained is about 20 keV, in reasonable agreement with the experiment.

In conclusion, we have observed betatron radiation from the interaction of a picosecond, relativistic $1 < a_0 < 3$ laser pulse with an underdense plasma. 2D OSIRIS PIC simulations show that betatron x-rays are explained by the emission from relativistic electrons accelerated primarily through SMLWFA. The number of betatron x-ray photons observed in our experiments ($10^9$ Photons/eV·Sr at 6 keV) is comparable to or better than the bremsstrahlung emission produced from foils at the same laser facility [30, 31]. It is also approaching the flux of high-Z-plasma M-band emission successfully used for single-shot x-ray absorption near edge structure (XANES) [32], a technique widely used to diagnose shock-compressed and warm dense matter [33–35]. Using betatron radiation to this end will greatly benefit from efficient x-ray focusing optics [36], x-ray spectrometer designs [37], and increased yield for kilojoule laser systems [9]. Hence, this first experimental demonstration of betatron x-ray emission in the SMLWFA regime is encouraging for undertaking future applications at larger-scale laser facilities.

This work was performed under the auspices of the U.S. Department of Energy under contract DE-AC52-07NA27344; supported by the Laboratory Directed Research and Development (LDRD) Program under tracking codes 13-LW-076 and 16-ERD-024 at LLNL, and by the joint NNSA/DOE program grant number DE-NA0002950 at UCLA. F.A. acknowledges support from the DOE Office of Science Early Career Research Program under SCW1575-1. R.W.F. acknowledges support from DOE Office of Fusion Energy Sciences under contract number DE-AC02-05CH11231. The authors thank R.C. Cauble, S. Andrews, B. Stuart, R. Costa, C. Bruns, C. Cadwalader and S. Maricle for their support of the Titan laser system at the Jupiter Laser Facility, J.J. Ruby and B. Galloway for help with earlier experiments, P. Michel and T. Ma for discussions on Ross pair filter analysis.

* albert6@llnl.gov
**Present address: Laboratory for Laser Energetics, 250 E River Rd, Rochester, New York 14623, USA

[1] S. Corde, K. T. Phuoc, G. Lambert, R. Fitour, V. Malka, and A. Rousse, Rev. Mod. Phys. **85**, 1 (2013).

[2] S. Fourmaux, S. Corde, K. T. Phuoc, P. Lassonde, G. Lebrun, S. Payeur, F. Martin, S. Sebban, V. Malka, A. Rousse, , and J. C. Kieffer, Optics Letters **36**, 2426 (2011).

[3] S. Kneip, C. McGuffey, F. Dollar, M. S. Bloom, V. Chvykov, G. Kalintchenko, K. Krushelnick, A. Maksimchuk, S. P. D. Mangles, T. Matsuoka, Z. Najmudin, C. A. J. Palmer, J. Schreiber, W. Schumaker, A. G. R. Thomas, and V. Yanovsky, Appl. Phys. Lett. **99**, 093701 (2011).

[4] J. Wenz, S. Schleede, K. Khrennikov, M. Bech, P. Thibault, M. Heigoldt, F. Pfeiffer, and S. Karsch, NATURE COMMUNICATIONS **6** (2015), 10.1038/ncomms8568.

[5] J. M. Cole, J. C. Wood, N. C. Lopes, K. Poder, R. L. Abel, S. Alatabi, J. S. J. Bryant, A. Jin, S. Kneip, K. Mecseki, D. R. Symes, S. P. D. Mangles, and Z. Najmudin, Scientific Reports **5**, 13244 EP (2015).

[6] J. Lindl, Physics of Plasmas **2** (1995).

[7] P. Sperling, E. J. Gamboa, H. J. Lee, H. K. Chung, E. Galtier, Y. Omarbakiyeva, H. Reinholz, G. Röpke, U. Zastrau, J. Hastings, L. B. Fletcher, and S. H. Glenzer, Phys. Rev. Lett. **115**, 115001 (2015).

[8] F. Albert and A. G. R. Thomas, Plasma Physics and Controlled Fusion **58**, 103001 (2016).

[9] J. Ferri, X. Davoine, S. Y. Kalmykov, and A. Lifschitz, Phys. Rev. Accel. Beams **19**, 101301 (2016).

[10] C. Joshi, T. Tajima, J. M. Dawson, H. A. Baldis, and N. A. Ebrahim, Phys. Rev. Lett. **47**, 1285 (1981).

[11] A. Modena, Z. Najmudin, A. E. Dangor, C. E. Clayton, K. A. Marsh, C. Joshi, V. Malka, C. B. Darrow, C. Danson, D. Neely, and F. N. Walsh, Nature **377**, 606 (1995).

[12] C. E. Clayton, K.-C. Tzeng, D. Gordon, P. Muggli, W. B. Mori, C. Joshi, V. Malka, Z. Najmudin, A. Modena, D. Neely, and A. E. Dangor, Phys. Rev. Lett. **81**, 100 (1998).

[13] D. Gordon, K. C. Tzeng, C. E. Clayton, A. E. Dangor, V. Malka, K. A. Marsh, A. Modena, W. B. Mori, P. Muggli, Z. Najmudin, D. Neely, C. Danson, and C. Joshi, Phys. Rev. Lett. **80**, 2133 (1998).

[14] M. I. K. Santala, Z. Najmudin, E. L. Clark, M. Tatarakis, K. Krushelnick, A. E. Dangor, V. Malka, J. Faure, R. Allott, and R. J. Clarke, Phys. Rev. Lett. **86**, 1277 (2001).

[15] A. Pukhov and J. Meyer-ter Vehn, Physics of Plasmas (1994-present) **5** (1998).

[16] C. Gahn, G. D. Tsakiris, A. Pukhov, J. Meyer-ter Vehn, G. Pretzler, P. Thirolf, D. Habs, and K. J. Witte, Phys. Rev. Lett. **83**, 4772 (1999).

[17] M. Adachi, E. Miura, S. Kato, K. Koyama, S. ichi Masuda, T. Watanabe, H. Okamoto, A. Ogata, and M. Tanimoto, Japanese Journal of Applied Physics **45**, 4214 (2006).

[18] J. Vieira, R. A. Fonseca, W. B. Mori, and L. O. Silva, Phys. Rev. Lett. **109**, 145005 (2012).

[19] S. P. D. Mangles, B. R. Walton, M. Tzoufras, Z. Najmudin, R. J. Clarke, A. E. Dangor, R. G. Evans, S. Fritzler, A. Gopal, C. Hernandez-Gomez, W. B. Mori, W. Rozmus, M. Tatarakis, A. G. R. Thomas, F. S. Tsung, M. S. Wei, and K. Krushelnick, Phys. Rev. Lett. **94**, 245001 (2005).

[20] S. Kneip, S. R. Nagel, C. Bellei, N. Bourgeois, A. E. Dangor, A. Gopal, R. Heathcote, S. P. D. Mangles, J. R. Marquès, A. Maksimchuk, P. M. Nilson, K. T. Phuoc, S. Reed, M. Tzoufras, F. S. Tsung, L. Willingale, W. B. Mori, A. Rousse, K. Krushelnick, and Z. Najmudin, Phys. Rev. Lett. **100**, 105006 (2008).

[21] C. E. Clayton, J. E. Ralph, F. Albert, R. A. Fonseca, S. H. Glenzer, C. Joshi, W. Lu, K. A. Marsh, S. F. Martins, W. B. Mori, A. Pak, F. S. Tsung, B. B. Pollock, J. S. Ross, L. O. Silva, and D. H. Froula, Phys. Rev. Lett. **105**, 105003 (2010).

[22] F. Albert, B. Pollock, J. Shaw, K. A. Marsh, J. E. Ralph, Y. H. Chen, D. Alessi, A. Pak, C. E. Clayton, S. H. Glenzer, and C. Joshi, Phys. Rev. Lett. **111**, 235004 (2013).

[23] C. D. Chen, J. A. King, M. H. Key, K. U. Akli, F. N. Beg, H. Chen, R. R. Freeman, A. Link, A. J. Mackinnon, A. G. MacPhee, P. K. Patel, M. Porkolab, R. B. Stephens, and L. D. V. Woerkom, Rev. Sc. Instr. **79**, 10E305 (2008).

[24] B. R. Maddox, H. S. Park, B. A. Remington, N. Izumi, S. Chen, C. Chen, G. Kimminau, Z. Ali, M. J. Haugh, and Q. Ma, Rev. Sc. Instr. **82**, 023111 (2011).

[25] E. Esarey, B. A. Shadwick, P. Catravas, and W. P. Leemans, Phys. Rev. E **65**, 056505 (2002).

[26] F. Albert, B. B. Pollock, J. L. Shaw, K. A. Marsh, J. E. Ralph, Y.-H. Chen, D. Alessi, A. Pak, C. E. Clayton, S. H. Glenzer, and C. Joshi, Plasma Physics and Controlled Fusion **56**, 084016 (2014).

[27] N. Lemos, J. L. Martins, F. S. Tsung, J. L. Shaw, K. A. Marsh, F. Albert, B. B. Pollock, and C. Joshi, Plasma Physics and Controlled Fusion **58**, 034018 (2016).

[28] J. Martins, S. Martins, R. Fonseca, and L. Silva, in *Harnessing Relativistic Plasma waves as Novel Radiation Sources from Terahertz to X-rays and Beyond*, Proc. SPIE, Vol. 7359, edited by A. R. Dino A. Jaroszynski (2009) pp. 73590V–1–73590V–8.

[29] J. Shaw, N. Lemos, K. Marsh, F. Tsung, W. B. Mori, and C. Joshi, Plasma Physics and Controlled Fusion **58**, 034018 (2016).

[30] C. D. Chen, P. K. Patel, D. S. Hey, A. J. Mackinnon, M. H. Key, K. U. Akli, T. Bartal, F. N. Beg, S. Chawla, H. Chen, R. R. Freeman, D. P. Higginson, A. Link, T. Y. Ma, A. G. MacPhee, R. B. Stephens, L. D. Van Woerkom, B. Westover, and M. Porkolab, Physics of Plasmas **16**, 082705 (2009), http://dx.doi.org/10.1063/1.3183693.

[31] L. C. Jarrott, A. J. Kemp, L. Divol, D. Mariscal, B. Westover, C. McGuffey, F. N. Beg, M. Suggit, C. Chen, D. Hey, B. Maddox, J. Hawreliak, H.-S. Park, B. Remington, M. S. Wei, and A. MacPhee, Physics of Plasmas **21**, 031211 (2014), http://dx.doi.org/10.1063/1.4865230.

[32] A. Lévy, F. Dorchies, M. Harmand, C. Fourment, S. Hulin, O. Peyrusse, J. Santos, P. Antici, P. Audebert, J. Fuchs, L. Lancia, A. Mancic, M. Nakatsutsumi, S. Mazevet, V. Recoules, P. Renaudin, and S. Fourmaux, Plasma Physics and Controlled Fusion **51** (2009), 10.1088/0741-3335/51/12/124021.

[33] A. Benuzzi-Mounaix, F. Dorchies, V. Recoules, F. Festa, O. Peyrusse, A. Lévy, A. Ravasio, T. Hall, M. Koenig, N. Amadou, E. Bambrink, and S. Mazevet, Phys. Rev. Lett. **107**, 165006 (2011).

[34] A. Lévy, F. Dorchies, A. Benuzzi-Mounaix, A. Ravasio, F. Festa, V. Recoules, O. Peyrusse, N. Amadou, E. Brambrink, T. Hall, M. Koenig, and S. Mazevet, Phys. Rev.

Lett. **108**, 055002 (2012).
[35] A. Denoeud, A. Benuzzi-Mounaix, A. Ravasio, F. Dorchies, P. M. Leguay, J. Gaudin, F. Guyot, E. Brambrink, M. Koenig, S. Le Pape, and S. Mazevet, Phys. Rev. Lett. **113**, 116404 (2014).
[36] F. Dorchies, N. Fedorov, and L. Lecherbourg, Review of Scientific Instruments **86**, 073106 (2015), http://dx.doi.org/10.1063/1.4926348.
[37] Y. Ping, D. G. Hicks, B. Yaakobi, F. Coppari, J. Eggert, and G. W. Collins, Review of Scientific Instruments **84**, 123105 (2013), http://dx.doi.org/10.1063/1.4841935.